Chapter 3

Interaction of saccharide ligands with extra-cellular sialic acid residues

Chapter 3. Interaction of saccharide ligands with extra-cellular sialic acid residues

Drug-resistance makes cancer untreatable disease hence, intensifying the need for drug development with identification of potential drug targets. This task is important yet a very difficult task. To pursue drug target identification and development, in the present work, multicomplex-based drug identification approach is employed.

3.1 Introduction

Post-translational modifications are essential for protein folding, stability, and function [1]. There are total five post-translational modifications namely, Acetylation [2,3], Amidation [4,5], Carboxylation [6], Glycosylation [7] and Phosphorylation [8,9]. Among all these post-translational modifications, Glycosylation is most complex from the perspective of chemical heterogeneity of modifications because, it involves the covalent attachment of sugar moieties to proteins. Cell surface proteins play a crucial role in the effective communication between the cell and its environment. These proteins are elaborated as N-linked glycans which take part in the Glycosylation pattern and play an important role in several biological functions such as, immune defense, fertilization, viral replication, parasitic infection, cell growth, inflammation, and cell-cell adhesion. Glycosylation pattern is not template-driven and is impossible to predict easily. Five classes of Glycosylation patterns have been produced by reaction of carbohydrate group with other functional group [10]. Thus, it is not surprising that Glycosylation changes are universal feature of malignant transformation and tumor progression among the cells [11, 12, 13]. This is evident from the increment in the branching of N-linked glycans thus, generating supplementary sites for terminal Sialic Acid (SA) residues. The sialic acid family includes 43 derivatives of the nine-carbon sugar neuraminic acid. The most common member of this group is N-acetylneuraminic acid (Neu5Ac or NANA). The over expression of sialyltransferases ultimately leads to hyper-sialylation along the exterior region of the cell [14]. SA occurs in several tumor-related carbohydrate antigens facilitating the cancer cells to detach from primary tumour and initiate metastasis [15].

Contemporary studies indicate towards the association between tumour growth and aberrant sialylation on a transcriptional level [16]. Moreover, during metastasis over-expression of SA on malignant colonic cells and tissues is quite evident [17]. The negative charge carried SA placed on cell surface is greater in several types of transformed cells [18, 19, 20]. Also, SA has amino function at 5^{th} position which indicates towards indirect contact with surrounding proteins. There is a lack of well-defined protocol to identify the reaction, such as, the accumulation of Neu5Ac in cells that do express it. Over the year's, aberrant expression of certain glycan structures have attained the status of well-known markers for recognizing cancer cells. [21, 22]. Experimental data suggests that, certain carriers decorated with saccharides [22] or sugar-mimetics [23, 24] exhibit high affinity towards over-expressed SA and galectin residues on cancer cell surface [17, 25, 26] yet, there is a dearth of supportive theoretical reports exploring these interactions.

In this chapter, we incorporate the saccharides (Galactose, Gal; Mannose, Man) and Boronated sugar mimetic molecule (Phenylboronic Acid, PBA) to recognize the concentration of SA on the carrier surface through using the state-of-the-art Density Functional Theory (DFT).[23, 27]. While, Tiwari et. al. verified (experimentally) the dual approach of, cationization and attachment of recognition peptide on the target the colon cancer cells which exhibit metastasis based on the expression of SA [28]. It was observed that, treatment of cells with neuraminidase resulted in a significant decline in the cellular uptake of nanoparticles, thus discerning a definitive role of over-expressed SA in the cell-nanoparticle interaction [28]. Over the past few decade's atomistic simulations using state-of-the-art DFT have been an effective and reliable tool to investigate chemical reactions guiding the prediction and interpretation of complex atomic behavior.

3.2 Materials and Methods

3.2.1 Selection and preparation of protein-ligand complexes

The monomer molecules such as drug molecules and target molecule were obtained from the literature (23, 26, 27). Two saccharides, Galactose (Gal) and Mannose (Man), and one sugar mimetic Phenylboronic Acid (PBA) are the choice of drug candidates. Optimization and relaxation process were performed by the ground state energy calculation using the code GAUSSIAN 09 [29]. Gradient-corrected DFT with three parameter functions (B3) was utilized for the calculation of Lee-Yang-Parr (LYP) correlation function [30, 31]. Atomic charge, bond calculation, vibrational frequencies and energy of the optimized structures were obtained through B3-LYP. In order to investigate the influence of physiological environmental on the drug resistivity, the targeted drugs were subjected to different pH and temperature environments. The corresponding binding energy was calculated using JAGUAR tool of SCHRODINGER suite (Version 4.7) [32].

The theoretical descriptions for pH calculations were established by Liptak and Shields [33] which take into account the pH environment in DFT calculations. The theoretical description for pH calculations provided by Liptak and Shields (2001) is implemented in the JAGUAR tool. Here, we briefly describe the theoretical formulation, which takes account of pH environment in the DFT calculations.

$$pKa = a\ pKa_{raw} + b \tag{3.1}$$

Where, Ka is the dissociation constant, which explains the quantitative measurement of the strength of acid in solution, p indicates -log of the value, a and b are empirical parameters [33, 34] and $pKa_{raw} = \frac{\Delta G}{2.3RT}$. Where, pKa_{raw} is the predicted value by the thermodynamic cycle and the experimental pKa ΔG is the free energy for deprotonation of the solution, R is

the universal gas constant, and T is temperature. The free energy is approximated by combining the gas phase and solution phase of total DFT energies for the protonated and deprotonated forms of the drug molecule. The free energy for the deprotonation of the solution is given by:

$$_{\Delta}G = E(A^{-})g - E(AH)g - E(AH)solv + E(A^{-})solv + Const \quad (3.2)$$

Where, E(A^{-})g is the gas phase DFT energy of protonated form, $E(AH)g$ is the gas phase energy of protonated form, $E(AH)solv$ is the Solvation energy of the protonated form and $E(A^{-})solv$ is solvation energy of the deprotonated form. Moreover, to the correct barrier height for basis set superposition error, we incorporate the Basis Set Superposition Error (BSSE) of intermolecular potential function before taking the data for further calculations by Boys-Bernardi counterpoise method [35]. Stability of the molecules emerges from the hyper-conjugative interactions. Where interaction energy E_{AB}^{opt} of the receptor and ligand molecule are calculated as the difference between energy of the complex and summation of the ligand and receptor energy separately,

$$E_{int}^{AB} = E_{AB}^{opt} - (E_{A}^{opt} + E_{B}^{opt}) + E_{AB}^{BSSE} \quad (3.3)$$

For elementary interpretation of the static structure, Frontier Molecular Orbital (FMO) was employed which is based on the concepts of Molecular Orbital (MO) theory and has been applied to the elementary interpretation of static structures [36]. The nature and magnitude of FMO interactions are postulated to be an indication of the activation energy for a reaction step to which they are relevant. Hyper-polarizability has also been calculated to reveal the isosurfaces and individual contribution of the molecules. The Highest Occupied Molecular Orbital (HOMO), Lowest Unoccupied Molecular Orbital (LUMO) and energy gap (ΔE) were also determined. HOMO and LUMO parameters govern the molecular interactions. To justify

the reactivity, global hardness (η) {eq. 3.4}[37], softness (σ) {eq. 3.5}[37], chemical potential (μ) {eq. 3.6}[38], nucleophilicity (N) [39], electrophilicity (ω) {eq. 3.7}[39] and electro-negativity (χ) [40] of the molecule were calculated as follows:

$$\eta = \frac{1}{2}(\in_{LuMO} - \epsilon_{HOMO}) \tag{3.4}$$

$$\sigma = \frac{1}{2}\eta \tag{3.5}$$

$$\mu = -\chi = \frac{1}{2}(\in_{HOMO} + \in_{LUMO}) \tag{3.6}$$

$$\omega = \frac{\mu^2}{2\eta} \tag{3.7}$$

Where, $\in_{LuMO}$ is the energy of lowest unoccupied molecular orbital and ϵ_{HOMO} is energy of highest occupied molecular orbital. Fukui function (FF) is a predictor of chemical condensed reactivity [37] which specifies the ionization potential and electron affinity (nucleophilicity versus electrophilicity). The corresponding FFs were calculated as follows [41] :

$$f^{+}(r) = \rho N + 1(r) - \rho N(r) \quad \text{(Nucleophilic attack)} \tag{3.8}$$

$$f^{-}(r) = \rho N(r) - \rho N - 1(r) \quad \text{(Electrophilic attack)} \tag{3.9}$$

$$f^{0}(r) = \rho N(r) \quad \text{(Radical attack)} \tag{3.10}$$

Where, ρN+1, ρN and ρN-1 represent the electron density of anionic, neutral and cationic residues, respectively. Considering the negative charge on sialic acid, we perform Mulliken population analysis to describe the probability of electrostatic interactions [42]. The charge density at a point r was then expressed in terms of the density matrix P as follows:

$$f^{+(k)} = \mathrm{q}k(N+1) - \mathrm{q}k(N) \quad \text{(Nucleophilic attack)} \tag{3.11}$$

$$f^{-(k)} = \mathrm{q}k(N) - \mathrm{q}k(N-1) \quad \text{(Electrophilic attack)} \tag{3.12}$$

$$f^{0(k)} = \frac{1}{2}(\mathrm{q}k(N+1) - \mathrm{q}k(N-1) \quad \text{(Radical attack)} \tag{3.13}$$

Here, qk (N), qk(N+1) and qk(N-1) are the Mulliken charges at atom k of the neutral, anion and cation species, respectively.

$$f^2(r) = \Delta f(r) \approx \rho N + 1(r) - \rho N - 1(r) - 2\rho N(r)$$
$$= f^+(r) - f^-(r) \quad (3.14)$$

The $\Delta f(r)$ above describes the stabilizing and destabilizing interactions between nucleophile and electrophile which helps in distinguishing the nucleophilic/electrophilic nature of a specific site within molecule [41]. The donor-acceptor interaction during complex formation was calculated with the help of second order perturbation theory [43]. In order to understand various second order interactions between filled orbital of one subsystem and vacant orbital of another subsystem, we have performed the Natural bond orbital (NBO) calculation [43]. NBO analysis possesses the role of intramolecular orbital interaction by the charge transfer in the complex. Second-order perturbation theory based NBO calculations consider the interaction between, filled donor and empty acceptor NBOs and their dynamics. For each donor (i) and acceptor (j) NBO the second order stabilization energy $E^{(2)}$ associated with electron delocalization is estimated as

$$E^{(2)} = q_i \frac{(F_{ij})^2}{\varepsilon_j - \varepsilon_i}, \quad (3.15)$$

Where, q_i is the orbital occupancy, ε_j and ε_i are diagonal elements and $F_{ij}$is off-diagonal NBO Fock matrix elements [43]. In addition to electrostatic forces, hydrogen bonding also plays a crucial role in maintaining the complex stability. Therefore, we analyze the effect of hydrogen bonding in the ligand–SA interaction by providing vibrational assignments to the interacting groups obtained from DFT.

3.3 Results and discussion

Table 3.1 shows that, the HOMOs with negative energy and LUMOs with positive energy are related to the ionization potential and electron affinity with typical approximations [44]. Variation of energy gap between the orbit inside the receptor and ligand pocket decides the interaction potential and repulsion affinity. Moreover, the gap between HOMO and LUMO determines reactivity of the site [44], where smaller gap indicates high charge transfer ability. From the table it is evident that the low and high pH results in undesirable behavior.

Table 3.1: Summary of calculated individual descriptors, HOMO, LUMO, energy gap, hardness, softness and chemical potential, of Gal-SA complex under different temperature and pH conditions.

pH	Temperature (˚C)	HOMO (eV)	LUMO (eV)	HLG (HOMO LUMO Gap)(eV)	Hardness (η) (eV)	Softness (σ) (eV)	Chemical Potential (μ) (eV)	Electrophilicity (ω) (eV)
5.0	37	-0.24060	-0.00975	0.23085	0.115425	4.232804	-0.125175	-0.06787
	42	-0.23824	-0.01139	0.22685	0.113425	4.408199	-0.124815	-0.06867
5.5	37	-0.24076	-0.01044	0.23032	0.11516	4.341785	-0.1256	-0.06849
	42	-0.24078	-0.00818	0.23260	0.1163	4.299226	-0.12448	-0.06661
6.0	37	-0.23584	-0.01229	0.22355	0.111775	4.473272	-0.124065	-0.06885
	42	-0.23484	-0.01187	0.22297	0.111485	4.484908	-0.123355	-0.06824
6.5	37	-0.24057	-0.01063	0.22994	0.11497	4.348961	-0.1256	-0.06860
	42	-0.24084	-0.01070	0.23014	0.11507	4.345181	-0.12577	-0.06873
7.0	37	-0.23763	-0.00813	0.22950	0.11475	4.357298	-0.12288	-0.06579
	42	-0.23614	-0.01023	0.22591	0.112955	4.426542	-0.123185	-0.06717

At pH of 6.0 the hyperthermic condition results in a maximum binding affinity. HOMO (electron donor), LUMO (electron acceptor), band gap, chemical potential (μ), absolute hardness (η), softness (σ) and reaction with respect to pH and thermal variations were calculated using DFT. There is additional bonding holding the atoms together. While a sigma bond is always the first bond between two atoms, a Π bond is always the second bond between two atoms. The intra-molecular interactions determine the Π*(anti-bonding molecular orbital) interaction between C_{22}-O_{23} atoms at receptor and ligand pocket site of SA and GAL orientation. Such Π* interactions stabilize the binding of the receptor and ligand pocket. In essence, such complexes indicate that, the geometry of Π-Π interactions is controlled by electrostatic contribution. Model of charge distribution suggests that, the donor-acceptor concept can be misleading when used to describe the Π-Π interactions. It is the property of the atoms in the regions of intermolecular contact that actually control the strength and geometry of interactions, rather than the overall molecular oxidation or reduction potential.

Table 3.2: Calculated Binding energy and distance between two optimized molecules with distinct pH and temperature after BSSE correction.

pH	**Temperature (˚C)**	**BSSE (kcal/mol)**	**$E_{binding}$ (kcal/mol)**	**Distance (Å)**
5.0	37	11.95	-14.55	1.75
	42	9.24	-26.22	1.77
5.5	37	11.91	-14.58	1.78
	42	7.37	-19.94	1.73
6.0	37	11.92	-14.55	2.03
	42	8.06	-26.52	1.67
6.5	37	7.35	-17.41	1.80
	42	7.37	-19.92	1.76
7.0	37	11.21	-19.24	1.73
	42	9.77	-15.79	2.21

Calculated data show that, the binding energy increases at 42°C relative to normal physiological temperature. Moreover, the refinement of binding affinity from -26.52 kcal/mol to -14.55 kcal/mol at 37°C is evident at pH 6.0, which indicates a 12 kcal/mol difference from the conditions at 37°C to 42°C in the tumour environment. This refinement appears to be much stronger than the one which could be expected experimentally. Besides, the correlation of distance with hyperthermia (42°C) and physiological pH (7.0) to 1.67 Å is evident. The effect of temperature is quite obvious in reduction of the donor binding energy in all the cases as seen in Table 3.2. The effective Coulomb interaction between the charges increase as the temperature is increased. In this case, the binding affinity starts to reduce with increase in pH. Overall, our observations suggest that, (i) increasing the temperature and decreasing pH, in general, have a favorable effect on binding affinity between SA and GAL, and (ii) induction of hyperthermia at tumour-relevant pH offers pronounced enhancement in the binding affinity. All calculations are well supported by the quantitative analysis of the experimental data [26]. Our findings resolve the long-standing question regarding drug formulations in acidic pH which show improved targeting ability and efficacy in animal models [45, 46]. Generally, as the binding energy increases, the bond length decreases, but here in some cases bond length and binding energy decrease simultaneously indicating that, the repulsive forces are prominent. Table 3.2 clearly indicates that, the bond length between interacting molecules is due to the hydrogen bond. [47]. Highest bond length was observed at 7.0 pH and 42°C (figure 3.1), However, this pH condition is unrealistic for a solid tumor microenvironment.

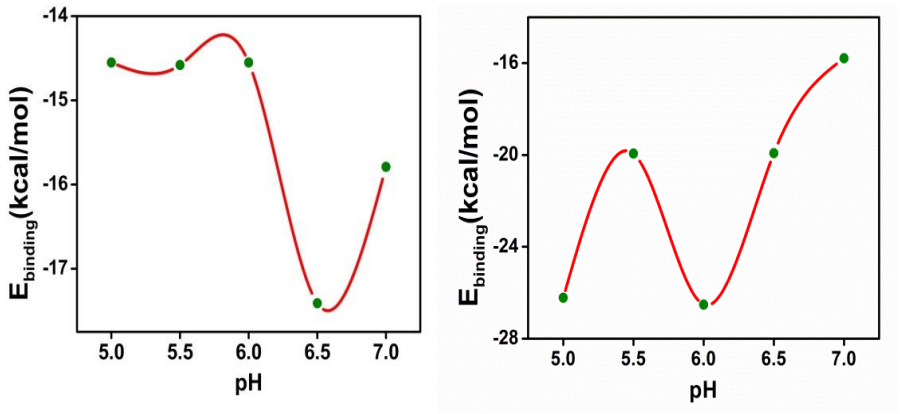

Figure 3.1: DFT calculated the binding energy curve of SA-Gal complex at 37˚C (a) and 42˚C (b) temperature and under various pH conditions.

Predominant of the non-covalent interactions such as, hydrogen bond, electrostatic, hydrophobic and van der Waals' were the contributors in the binding energy distributers of our study. However, the binding constants are typically around 103–104 M^{-1}. This is weaker

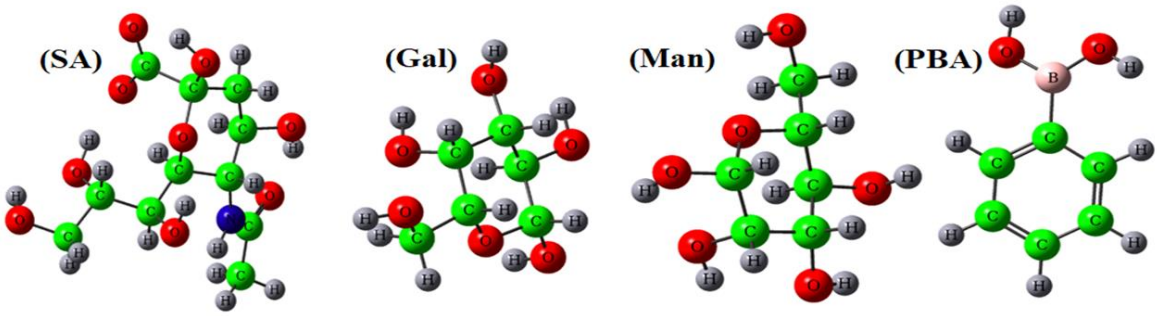

Figure 3.2: Molecular structure of target oligo-saccharide SA and ligand saccharides Monovalent Gal, Man and PBA carries the Carbon (C) with parrot green color, Oxygen (O) is in red, Hydrogen (H) is in grey and Nitrogen (N) is in blue and Boron is in peach color

as compared to the bio-recognition events. Multi-valency is actually a key working principle of molecular recognition in biological systems, which makes cumulative use of individually weak interactions. Multivalent saccharide binding are known to enhance both, the affinity and selectivity [25, 48].We architect the extra branch on the ligands as bi-valency to enhance the interaction affinity with target residue as shown in Table 3.3. Figure 3.2 represents the atomic structure of SA as a target residue and ligands GA, MAN and PBA. GAL-SA monovalent complex achieves a strong binding affinity of -31.7353 kcal/mol with 0.0289 HLG with respect to MAN-SA and PBA-SA. Moreover, their bivalent configuration shows minor

interactions with SA as compared to MAN and PBA which is contradictory to the literature [25]. Chen et. al. [49] observed the effect of numbers of optimal MAN unit per nano carriers (NC) and the distance between mannose units upon NC uptake in macrophage cells. A decline in the uptake was observed beyond two MAN units per NC. Clustering of membrane receptors in association with higher MAN units impeded their engagement with NC. Occupancy of ligands receptor binding domain as a function of their inter-atomic and spacer distances can also affect the orientation of ligand under appropriate entropic configuration. Another contradictory result was related to monovalent SA-PBA interaction. [49]

Table 3.3: Computed binding energy as well as molecular orbits of ligands under mono- and bi-valent configurations with target molecule.

Interaction complex	**Configuration of ligand**	**$E_{binding}$(kcal/mol)**	**HOMO**	**LUMO**	**HLG**
Gal-SA	Monovalent	-31.7353	-0.1242	-0.0953	0.0289
	Bivalent	49.8781	-0.1926	-0.0366	0.1559
Man-SA	Monovalent	-23.8794	-0.1235	-0.0667	0.0568
	Bivalent	-54.9871	-0.0396	-0.1529	0.1926
PBA-SA	Monovalent	164.4198	-0.1083	-0.0572	0.0511
	Bivalent	-244.9476	-0.22545	-0.02079	0.20466

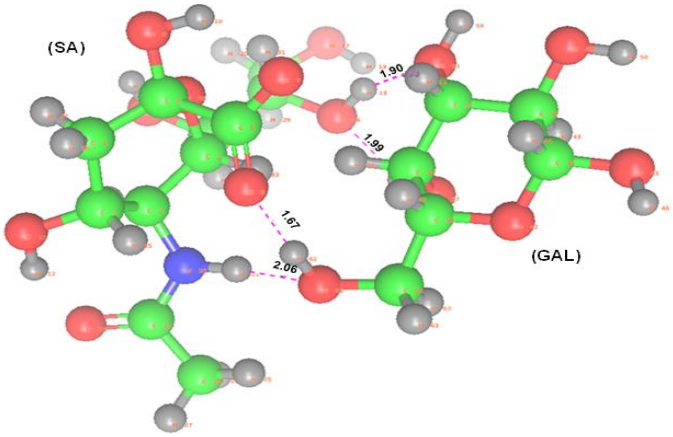

Figure 3.3: Optimized structure of SA-Gal with the least bond distance (d =1.67Å) between O8-H62 which belongs to targeted molecule and ligand molecule respectively.

The Fukui functions in the table 3.4, f +, represents the best way to change the electron density in response to an increase in the number of electrons; consequently, it can be employed to predict the preferred site for a nucleophilic attack. The Fukui function, f -, represents the best way to change the electron density in response to a decrease in the number of electrons; consequently, it can be employed to predict the preferred site for an electrophilic attack. Tabular data of Fukui function f(r) clearly depicts the complex reactivity.

Table 3.4: Electrophilicity and nucleophilicity of highly participated atoms in the reaction from Gal-SA complex.

Atoms	**f^+**	**f^-**	**f(r)**
C_6	0.0005	0.0636	-0.0631
O_8	0.0001	0.4842	-0.4841
N_{20}	0.1162	0.0002	0.1160
C_{22}	0.4890	-0.0000	0.4890
O_{23}	0.2015	0.0007	0.2008
O_{28}	0.0009	0.0920	-0.0911

System softness is indicated by the charge difference between electrophilic and nucleophilic atom and highlights the pocket site of the molecule. Interaction affinity and local softness of molecules are directly proportional to each other. Nucleophilic nature of molecule is promoting the local softness and increase the interaction affinity at atomic level. A comparison of a resultant series for the SA-GAL complex molecule for different acceptable point charge sizes showed , C_6, O_8, and O_{28} acted as primary nucleophilic whereas C_{22}, N_{20}, and O_{23} were primary electrophilic attack sites. The C_6, O_8 and O_{28} atoms of GAL are preferred site for an electrophilic attack (Table 3.4). Pictorial data in Figure 3.4 displays the charge distribution of complex in the range of -0.6315 to 0.585 a.u with involved atom in interaction. Highly neucleophilic is shown in purple and electrophilic carries in grey color. Oxygen atoms O_8 and O_7 from SA molecule possess highest negative charge -0.6315 as compared to others and appear as a nucleophilic acceptor. It shows the interaction with H_{62} of

Gal carried +0.3716 charge with resultant bond distance of 1.67 Å. A carboxylic acid at the C_6 position and various α-glycosidic linkages to the sugar chain stemmed from O_8 atom. The Mulliken charge is directly related to the vibrational properties of the molecule and quantifies how the electronic structure charges redistribute themselves under atomic displacements. Electronic interactions originate from the equal sharing of charge between two atoms. Therefore, it is related to the chemical bonds present in the molecule. It is critical to determine the hydrogen bonds between carbohydrate residues. [50, 51] since this interaction affects the dipole moment, polarizability, electronic structure and other properties of molecular system [52].

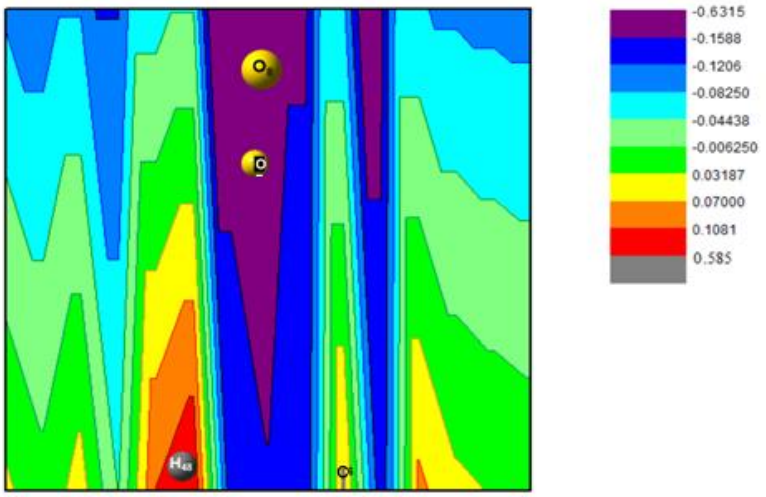

Figure 3.4: Calculated Mulliken atomic charge distribution (in atomic unit) throughout the SA-Gal complex.

The net atomic charge of SA molecule is negative. Taking this into account the point charge of SA and saccharide by means of Mulliken population analysis is represented in Fig. 3.4. The total charge of the molecule is equal to zero, the calculated results reveal that, the negative charge is delocalized in oxygen atoms.

The NBO hierarchy of bonding interactions begins with filled (donor) and vacant (acceptor) natural atomic orbitals, NAOs of each participating atom. Vacant valence-shell NAOs of atom 'A' may be conveniently distinguished with an asterisk (e.g., $\theta_K^{(A)}$) to denote their

acceptor character. NBO analysis is an efficient method for studying intra- and inter-molecular bonding along with the interaction among bonds. It also provides a convenient basis for investigation of charge transfer or conjugative interactions in molecular system [53]. Some electron donor orbital, acceptor orbital and the interacting stabilization energy resulting from the second order micro-disturbance theory have been previously reported [54, 55, 56, 57]. The larger the (E^2) value, the more intensive is the interaction between electron donors and the greater the extent of conjugation of the whole system. Delocalization of electron density between occupied Lewis type (bond or lone pair) NBO orbitals and formally unoccupied (anti-bonding or Rydberg) non-Lewis NBO orbital's correspond to stabilization of the donor-acceptor interaction. The molecular interaction is formed by the orbital overlap between σ and σ* orbitals which results in intra-molecular charge transfer (ICT) leading to the stabilization of the system. Since the equilibrium energy (E^2) is related with the stabilization strength of the two orbitals with electron donor as *i* and acceptor as *j* as shown in Table A1 in Appendix. The strong intra-molecular hyper-conjugative interaction of C_6-O_8 from O_7 with LP (2) orbital → π* (N_6-C_8) which increases electron density (ED) (0.05474) (as represented in Table 5) that weakens the bonds leading to stabilization with binding energy of 22.18 kJ/mol Natural hybrid orbital LP (2) from O8 to σ*C6-O7, which occupies a higher energy orbital (0.37035a.u.) with considerable 97.72 kJ/mol binding energy and low occupation number (1.88814a.u.). Since, the valance electronic configurations and occupancy of O_7, O_8 and O_9 atoms are $^2s^2p$ (5.00), $^2s^2p$ (5.08) and $^2s^2p$ (5.09), respectively it indicates that, the involvement of single unpaired electron and the role of sp hybridization. Where, other orbitals with higher hyper-conjugative interactions are LP(2)O_7; π*C_6-O_8, LP(2)O_{23}; σ*C_{22}-O_{24}, and LP(2)O_9; σ*C_5-O_{28}.

Table 3.5: FT-IR, Raman activity, Vibrational bonds, and their assignment for target molecule SA and ligand molecule Galactose with different Frequencies.

Frequency cm^{-1}	**Observed bands**	**Vibrational Bond (SA)**	**Assignments (SA)**	**Vibrational Bond (Galactose)**	**Assignments (Galactose)**
3483	385^{IR}	H(21)-N(20)	Antisymmetric	H(62)-O(61)	Rocking
3352	649^{IR}	H(21)-N(20)	Rocking	H(62)-O(61)-C(59)	Rocking
1597	258^{IR}	C(22)-N(22)-H(21)	antisymmetric	H(62)-O(61)	Rocking
1497	179^{IR}	C(14)-O(16)-O(18)	Rocking	C(55)-O(57)-H(58)	Scissoring
1474	52^{R}	C(14)-O(16)-O(18)	Rocking	C(55)-O(57)-H(58)	Scissoring
1470	21^{R}	C(14)-O(16)-O(18)	Rocking	C(55)-O(57)-H(58)	Scissoring
1444	87^{IR}	H(18)-O(16)-C(14)	Rocking	C(55)-H(56)	antisymmetric
1434	33^{IR}	H(18)-O(16)-C(14)	Rocking	C(51)-C(55)-H(56)	Scissoring
1422	87^{R}	H(34)-C(2)-N(20)	Rocking	H(62)-O(61)-C(59)	Scissoring
1416	22^{R}	C(4)-C(2)-N(20)	Antisymmetric	C(40)-C(59)	Rocking
1412	59^{IR}	H(21)-N(20)-C(22)	Rocking	C(59)-O(61)-H(62)	Rocking
1377	8^{IR}	H(18)-O(16)-C(14)	Rocking	H(58)-O(57)-C(55)	Rocking
1357	100^{IR}	H(18)-O(16)-C(14)	Rocking	H(58)-O(57)-C(55)	Rocking
1352	100^{IR}	O(16)-C(14)	antisymmetric	H(58)-O(57)-C(55)	Rocking
1346	33^{IR}	C(24)-C(22)-N(20)	antisymmetric	O(61)-H(62)	antisymmetric
1337	35^{R}	H(18)-O(16)	Antisymmetric	H(58)-O(57)-C(55)	Rocking
1328	39^{IR}	C(22)-N(20)-H(21)	Antisymmetric	H(58)-O(57)-C(55)	Rocking
1318	105^{R}	C(22)-N(20)-H(21)	Rocking	H(62)-O(61)-C(59)	Rocking
1307	75^{R}	C(22)-N(20)-H(21)	Antisymmetric	H(62)-O(61)-C(59)	Rocking
1287	21^{R}	C(2)-N(20)	Rocking	H(62)-O(61)-C(59)	Rocking
1270	20^{IR}	C(2)-N(20)	Rocking	H(62)-O(61)-C(59)	Rocking
1244	29^{R}	C(2)-N(20)-	Antisymmetric	H(62)-O(61)-	Rocking

		H(21)		C(59)	
1238	30^{IR}	C(2)-N(20)-H(21)	Rocking	H(62)-O(61)-C(59)	Rocking
1230	23^{IR}	H(31)-C(14)-O(16)	Scissoring	C(55)-O(57)-H(58)	Rocking
1227	28^{IR}	O(11)-N(20)-H(21)	Rocking	O(61)-C(59)	Rocking
1167	52^{IR}	C(2)-N(20)-H(21)	Rocking	H(62)-O(61)-C(59)	Rocking
1149	28^{IR}	H(33)-C(1)-C(2)	Scissoring	H(63)-C(59)-O(61)	Scissoring
1142	11^{R}	C(14)-C(13)-C(1)	Scissoring	H(58)-O(57)-C(57)	Rocking
1124	30^{IR}	N(20)-C(5)-C(1)	Antisymmetric	C(40)-C(59)	Antisymmetric
1118	51^{IR}	C(5)-C(1)	Antisymmetric	C(59)-O(61)	Antisymmetric
1109	340^{IR}	N(20)-C(5)-C(1)	Antisymmetric	C(40)-C(59)-O(61)	Antisymmetric
1102	59^{IR}	N(20)-C(2)-C(1)	antisymmetric	C(40)-O(42)	antisymmetric
1099	29^{IR}	C(22)-C(24)-H(24)	Scissoring	C(40)-C(59)-O(61)	Antisymmetric
1081	79^{IR}	C(22)-C(24)-H(27)	Scissoring	H(41)-C(40)-O(42)	Rocking
1078	53^{IR}	O(16)-C(14)-C13	Antisymmetric	H(58)-O(57)-C(56)	Rocking
1068	53^{IR}	C(24)-C(22)	Antisymmetric	H(52)-C(55)-H(56)	Rocking
1046	119^{IR}	C(2)-N(20)-H(21)	Rocking	H(56)-C(55)-C(51)	Rocking
1042	57^{IR}	H(26)-C(24)-H(25)	Rocking	O(61)-C(59)-H(60)	Rocking
955	14^{IR}	O(23)-C(22)-N(20)	Scissoring	O(61)-C(59)-H(63)	Rocking
930	48^{IR}	N(20)-C(2)-C(3)	Rocking	O(61)-C(59)-H(40)	Twisting
830	22^{IR}	C(2)-N(20)-H(21)	Scissoring	H(62)-O(61)-C(59)	Rocking
799	24^{IR}	C(2)-N(20)-H(21)	Rocking	H(62)-O(61)-C(59)	Twisting
787	103^{IR}	C(5)-C(6)-H(21)	Rocking	H(62)-O(61)-C(59)	Rocking
748	63^{IR}	N(20)-H(21)	Antisymmetric	O(61)-H(62)	antisymmetric
747	106^{IR}	C(2)-N(20)-H(21)	Rocking	H(41)-C(40)-C(55)	Rocking
		C(14)-O(16)	Antisymmetric	-	-
699	11^{R}	N(20)-H(21)	Antisymmetric	C(40)-C(55)	antisymmetric

625	30^{R}	O(11)-H(12)	Antisymmetric	C(43)-C(47)	antisymmetric
552	106^{IR}	C(15)-C(14)-C(16)	Rocking	H(58)-O(57)-C(55)	Rocking
526	49^{R}	H(19)-O(17)-O(15)	Rocking	O(47)-C(43)-C(47)	Scissoring
438	10^{R}	O(11)-C(3)-C(2)	Rocking	C(59)-C(40)-O(42)	Rocking
305	15^{IR}	N(20)-C(22)-C(24)	Scissoring	C(55)-O(57)-H(58)	Rocking
261	8^{R}	H(34)-C(2)-N(20)	Scissoring	O(61)-C(59)-H(60)	Scissoring
229	20^{IR}	C(4)-C(5)-C(6)	Rocking	O(61)-C(59)-C(40)	Rocking

The purpose of vibrational modes is the detailed investigation of the substituent effect on the vibrational spectra of complex (SA-GAL) using IR and Raman spectra followed by normal coordinate analysis. Vibrational assignments of fundamentals often made on the basis of the unscaled frequencies by assuming the observed frequencies so that they are in the same order as the calculated ones. The observed IR, Raman bands, calculated (scaled) wavenumbers and assignments are given in Table 3.5. The stretching vibrations of the NH group are expected in the range of 3000-3500 cm^{-1} frequency [58]**.** The asymmetric stretching modes of the amine group are calculated to be at 649 cm^{-1}, IR intensity at 3482 cm^{-1} with anti-symmetric (H_{21}-N_{20}) and 3352 cm^{-1} with rocking (H_{21}-N_{20}) vibrations. The N-H group is characterized by the bands at 1510-1500, 1350-1250 and 740-730 cm^{-1} [59]. Where, N- atom is from our target molecule which is clearly revealing modes after appearance of the ligand molecule GAL. The vibrations influenced by C-C bonds appear within the region of 1000 to 1300 cm^{-1}[58], based on experiments. In the present study, the vibrations in SA were observed at 1068 and 1118 cm^{-1} with antisymmetric (C_{24}-C_{22}) and (C_5-C_6) respectively in Raman bands. The galactose has been identified at 1124 cm^{-1} with antisymmetric (C_{40}-C_{59}) and 1416 cm^{-1} with rocking (C_{40}-C_{59}) vibrations. These results show that the theoretical values are in decent agreement with the experimental results. The O-C stretching modes are expected in range of

1000 to 1300 cm^{-1}. The bands assigned at 747 and 1352 cm^{-1} for O_{16}-C_{14} in SA molecule and 1118 cm^{-1} for C_{59}-O_{61} with antisymmetric on galactose. IR intensities of structure are 51, 100, and 106 respectively. Two FT-IR spectra peaks spotted at 53 and 57 cm^{-1} are assigned as the bending modes of HCH.

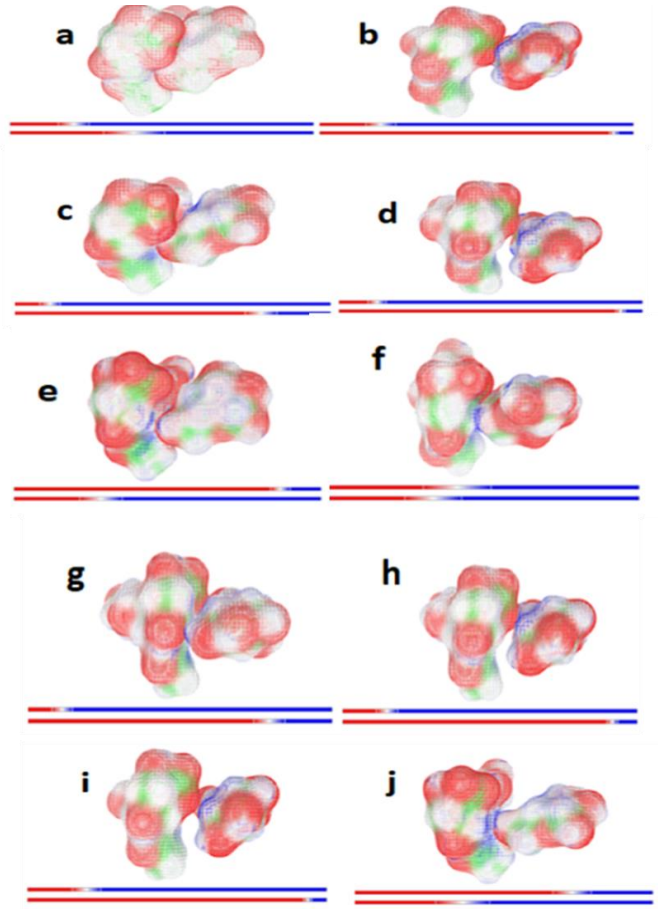

Figure 3.5: Density of electrons with red (high electron density (-))and blue (low electron density (+)) surface at different pH and temperature: (a) pH 5.0; 37˚C, (b) pH 5.0; 42˚C, (c) pH 5.5; 37˚C, (d) pH 5.5; 42˚C, (e) pH 6.0; 37˚C, (f) pH 6.0; 42˚C, (g) pH 6.5; 37˚C, (h) pH 6.5; 37˚C, (i) pH 7.0; 37˚C, and (j) pH 7.0; 42˚C.

In present study H-C-C bending is identified in the region 747 to 1434 cm^{-1} and 6 HCC vibrations of whole complex observed and spotted FT-IR spectra peaks are 33, 36, 79, 103, 106, and 119 cm^{-1}. Eleven H-C-N vibrations are examined in region 747 to 1597 cm^{-1}. Other bending vibrations such as NCC, OCC, COH, HOO, HCC and OCH are identified. Identified FT-IR peaks are at 22, 30, 39, 52, 68, 76, 103, 106, 119, and 258 cm^{-1}. The occurrences of these vibrations are around ten.

In order to predict the molecular reactive of the sites, another non-specific interaction parameter for the title compound (SA- GAL) is shown in Fig. 3.5. The molecular electrostatic potential (MEP) is a useful property to study the reactivity of the title compound towards electrophilic and nucleophilic attack [60-63]. Here we have included different values of electrostatic potential on the surfaces represented with different colors. Potential increases in the order red < orange < yellow < green < blue where, blue indicates the highest electrostatic potential energy and red indicates the lowest electrostatic potential energy. In the present study, highest electron density was expected at the receptor pocket site. Hence, highest negative and positive electrostatic potential appeared localized over the oxygen (O_8) and carbon (C_{22}) atoms, respectively. So, an approaching electrophile will be attracted to negative regions (mainly to points with most negative values), where the electron distribution effect is dominant. From the MEP it is evident that the negative charge covers the C=O groups and the positive region cover the rings and NH group.

Overall, we have adopted a simplistic approach to describe the interaction of a small molecule ligand with extracellular SA. Real targeted theranostic carrier systems are far more complex. Often, they are composed of macromolecular backbones appended with ligand units, often employing spacer molecules and with different degrees of substitution. Therefore, inclusion of carrier-related variables can make the model more realistic. For instance, we have not modeled the possibility of appending GAL over a polymer template, steric influence of pendant groups on Gal-SA interaction and the probability of pre-mature dissociation of GAL from the template under cancer-related physiological insults. In future, this approach will be updated to model a more realistic system through the application of a wider simulation box.

3.4 Conclusion

In this chapter, we have investigated the classical and quantum properties such as structural, molecular, vibrational and electronic properties for recognition of malignant surface cell in the form of SA content availability using monovalent saccharides. Moreover, we have confirmed the strong binding energy of three monovalent, three bi- valent and mimic ligand saccharides along with target molecule SA. All calculations were carried out within the framework of DFT.

Theoretical DFT and ab-initio calculations of the vibrational spectra of the molecule presented in this chapter were compared with the FTIR and Raman spectra. Initially, we investigated the binding properties of monovalent and bi-valent saccharides with SA and found that GAL carries good binding consistency than other monovalent and bi- valent saccharides and mimic. Once the interaction properties were confirmed, we incorporated the body environment factors such as various pH and temperature to spot the resistance and achieve the targeted drug therapy. Also we verify the targeted therapy for provided drug using vibrational spectroscopy because it is a non-destructive analytical method and we can check when it is associated with chemo metrics and makes the bond with various group of target. Body temperature of 37˚C and chemotherapeutical temperature of 42˚C have been included for each pH as 5.0, 5.5, 6.0, 6.5 and 7.0. From the binding energy, electronic properties and stability of the complex we arrive at the conclusion that, Galctose at hyperthermic condition and 6.0 pH shows the better stability.

Appendix

Table A1: Electron acceptor, donor percentage and bond type of each interacted atom of targeted and ligand molecules.

Donor(i) (occupancy)	Type	ED_A % ED_B %	Acceptor(j) (occupancy)	Type	ED_A % ED_B %	$E^{(2)a}$ (kcal/mol)	E_j-E_i^b (a.u.)	$F_{(ij)}^c$ (a.u.)
CR (1) C_1 1.99902	σ	-	BD* (1)C_1-O_{28} 0.02939	σ*	67.26 32.74	0.95	10.42	0.089
CR (1) C_1 1.99902	σ	-	BD* (1)C_5-O_{28} 0.10041	σ*	69.96 30.04	0.79	10.37	0.081
CR (1) C_2 1.99912	σ	-	BD*(1)N_{20}-C_{22} 0.06556	σ*	37.50 62.50	0.77	10.57	0.081
CR (1) C_3 1.99908	σ	-	BD* (1) C_3-O_{11} 0.02483	σ*	66.47 33.53	1.10	10.42	0.096
CR (1)C_5 1.99898	σ	-	BD* (1)C_1-O_{28} 0.02939	σ*	67.26 32.74	0.77	10.47	0.080
CR (1)C_5 1.99898	σ	-	BD* (1)C_4-C_5 0.03863	σ*	49.52 50.48	0.67	10.56	0.075
CR (1)C_5 1.99898	σ	-	BD* (1)C_5-O_{28} 0.10041	σ*	69.96 30.04	0.71	10.42	0.077
CR (1)C_5 1.99898	σ	-	BD* (1)O_9-H_{10} 0.05186	σ*	22.85 77.15	0.62	10.61	0.072
CR (1)O_7 1.99978	σ	-	BD* (1)C_6-O_8 0.05474	π*	66.80 33.20	0.83	19.42	0.113
CR (1)O_8 1.99971	σ	-	BD* (1)C_6-O_7 0.37035	σ*	66.38 33.62	0.88	19.44	0.116
CR C_{13} 1.99902	σ	-	BD*(1)C_{13}-O_{37} 0.02052	σ*	66.83 33.17	1.06	10.41	0.094
CR (1)C_{14} 1.99907	σ	-	BD*(1)C_{14}-O_{16} 0.03030	σ*	68.04 31.96	1.16	10.39	0.098
CR (1)C_{15} 1.99923	σ	-	BD*(1)C_{15}-O_{17} 0.01063	σ*	66.72 33.28	1.03	10.42	0.092
CR (1)N_{20} 1.99934	σ	-	BD*(1)C_{22}-O_{23} 0.04451	π*	65.90 34.10	0.62	14.71	0.086
CR (1)C_{22} 1.99939	σ	-	BD* (1)C_2-N_{20} 0.02675	σ*	62.16 37.84	1.24	10.52	0.102
CR (1)C_{22} 1.99939	σ	-	BD*(1)N_{20}-H_{21} 0.03952	σ*	26.41 73.59	0.76	10.65	0.080
CR (1)O_{23} 1.99977	σ	-	BD*(1)N_{20}-C_{22} 0.06556	σ*	37.50 62.50	0.62	19.36	0.098
CR (1)O_{23} 1.99977	σ	-	BD*(1)C_{22}-C_{24} 0.05333	σ*	51.46 48.54	0.67	19.24	0.102
CR (1)C_{24} 1.99937	σ	-	BD*(1)C_{22}-O_{23} 0.04451	π*	65.90 34.10	0.57	10.61	0.069

LP (1)O_7 1.97033	σ	-	BD* (1)C_5-C_6 0.12449	σ*	46.42 53.58	3.11	1.00	0.050
LP (1)O_7 1.97033	σ	-	BD* (1)C_6-O_8 0.05474	π*	66.80 33.20	1.19	1.23	0.034
LP (1)O_7 1.97033	σ	-	BD* (1)O_9-H_{10} 0.05186	σ*	22.85 77.15	2.62	1.11	0.048
LP (2)O_7 1.97033	σ	-	BD* (1)C_4-C_5 0.03863	σ*	49.52 50.48	0.67	0.63	0.018
LP (2)O_7 1.97033	σ	-	BD* (1)C_5-C_6 0.12449	σ*	46.42 53.58	16.52	0.58	0.087
LP (2)O_7 1.97033	σ	-	BD* (1)C_6-O_8 0.05474	π*	66.80 33.20	22.18	0.81	0.119
LP (2)O_7 1.97033	σ	-	BD* (1)O_9-H_{10} 0.05186	σ*	22.85 77.15	2.62	1.11	0.048
LP (1) O_8 1.93135	σ	-	BD* (1)C_3-H_{35} 0.03385	σ*	37.58 62.42	0.56	1.13	0.022
LP (1) O_8 1.93135	σ	-	BD* (1)C_5-C_6 0.12449	σ*	46.42 53.58	0.71	1.00	0.024
LP (1) O_8 1.93135	σ	-	BD* (1)C_6-O_7 0.05312	σ*	66.38 33.62	4.33	1.23	0.065
LP (2)O_8 1.88814	σ	-	BD* (1)C_3-O_{11} 0.02483	σ*	66.47 33.53	0.63	0.56	0.017
LP (2)O_8 1.88814	σ	-	BD* (1)C_3-H_{35} 0.03385	σ*	37.58 62.42	0.65	0.72	0.019
LP (2)O_8 1.88814	σ	-	BD* (1)C_5-C_6 0.12449	σ*	46.42 53.58	19.30	0.59	0.095
LP (2)O_8 1.88814	σ	-	BD* (1)C_5-O_9 0.03764	σ*	66.92 33.08	0.91	0.60	0.021
LP (2)O_8 1.88814	σ	-	BD* (1)C_6-O_7 0.05312	σ*	66.38 33.62	16.12	0.82	0.102
LP (2)O_8 1.88814	σ	-	BD* (2)C_6-O_7 0.37035	σ*	74.46 25.54	0.60	0.28	0.012
LP (3)O_8 1.88814	σ	-	BD* (2)C_6-O_7 0.37035	σ*	74.46 25.54	97.72	0.27	0.145
LP (1)O_9 1.97666	σ	-	BD* (1)C_5-C_6 0.12449	σ*	46.42 53.58	3.49	0.91	0.050
LP (2)O_9 1.905O_9	σ	-	BD* (1)C_1-O_{28} 0.02939	σ*	67.26 32.74	0.71	0.59	0.018
LP (2)O_9 1.905O_9	σ	-	BD* (1)C_4-C_5 0.03863	σ*	49.52 50.48	2.48	0.67	0.036
LP (2)O_9 1.905O_9	σ	-	BD* (1)C_5-C_6 0.12449	σ*	46.42 53.58	1.26	0.62	0.025
LP (2)O_9 1.905O_9	σ	-	BD* (1)C_5-O_{28} 0.10041	σ*	69.96 30.04	21.01	0.54	0.095
LP (1)O_{11} 1.97729	σ	-	BD* (1)C_2-C_3 0.04675	σ*	47.83 52.17	1.89	0.93	0.037

LP (1)O_{11} 1.97729	σ	-	BD* (1)C_3-C_4 0.02430	σ*	50.57 49.43	1.12	0.96	0.029
LP (1)O_{11} 1.97729	σ	-	BD* (1)C_3-H_{35} 0.033385	σ*	37.58 62.42	0.84	1.04	0.026
LP (2)O_{11} 1.95721	σ	-	BD* (1)C_2-C_3 0.04675	σ*	47.83 52.17	5.20	0.64	0.051
LP (2)O_{11} 1.95721	σ	-	BD* (1)C_3-H_{35} 0.033385	σ*	37.58 62.42	7.05	0.75	0.065
LP (1)O_{16} 1.96834	σ	-	BD*(1)C_{14}-H_{31} 0.02469	σ*	37.83 62.17	2.72	1.04	0.048
LP (1)O_{16} 1.96834	σ	-	BD*(1)O_{17}-H_{19} 0.02204	σ*	25.14 74.86	0.68	1.05	0.024
LP (2)O_{16} 1.93743	σ	-	BD*(1)C_{13}-C_{14} 0.04624	σ*	50.22 49.78	4.96	0.69	0.052
LP (2)O_{16} 1.93743	σ	-	BD*(1)C_{13}-O_{37} 0.02052	σ*	66.83 33.17	0.96	0.61	0.022
LP (2)O_{16} 1.93743	σ	-	BD*(1)C_{14}-C_{15} 0.04028	σ*	49.20 50.80	4.99	0.69	0.052
LP (2)O_{16} 1.93743	σ	-	BD*(1)C_{15}-H_{30} 0.01718	σ*	38.28 61.72	0.65	0.79	0.020
LP (2)O_{16} 1.93743	σ	-	BD*(1)O_{17}-H_{19} 0.02204	σ*	25.14 74.86	2.77	0.78	0.041
LP (1)O_{17} 1.98266	σ	-	BD*(1)C_{14}-C_{15} 0.04028	σ*	49.20 50.80	1.70	0.96	0.036
LP (1)O_{17} 1.98266	σ	-	BD*(1)C_{15}-H_{29} 0.03144	σ*	39.81 60.19	0.89	1.02	0.027
LP (1)O_{17} 1.98266	σ	-	BD*(1)C_{15}-H_{30} 0.01718	σ*	38.28 61.72	1.32	1.06	0.033
LP (2)O_{17} 1.95605	σ	-	BD*(1)C_{13}-C_{14} 0.04624	σ*	50.22 49.78	0.72	0.65	0.019
LP (2)O_{17} 1.95605	σ	-	BD*(1)C_{14}-C_{15} 0.04028	σ*	49.20 50.80	4.87	0.65	0.050
LP (2)O_{17} 1.95605	σ	-	BD*(1)C_{15}-H_{29} 0.03144	σ*	39.81 60.19	7.40	0.72	0.065
LP (1)N_{20} 1.67980	σ	-	BD* (1)C_1-C_2 0.3956	σ*	50.72 49.28	1.00	0.63	0.022
LP (1)N_{20} 1.67980	σ	-	BD* (1)C_1-O_{28} 0.02939	σ*	67.26 32.74	0.59	0.58	0.016
LP (1)N_{20} 1.67980	σ	-	BD* (1)C_2-C_3 0.04675	σ*	47.83 52.17	8.02	0.63	0.063
LP (1)N_{20} 1.67980	σ	-	BD* (1)C_2-H_{34} 0.02504	σ*	36.22 63.78	2.01	0.73	0.034
LP (1)N_{20} 1.67980	σ	-	BD* (1)C_3-C_4 0.02430	σ*	50.57 49.43	0.57	0.66	0.017
LP (1)N_{20} 1.67980	σ	-	BD*(1)N_{20}-H_{21} 0.03952	σ*	26.41 73.59	0.82	0.73	0.022

LP (1)N_{20} 1.67980	σ	-	BD*(1)C_{22}-O_{23} 0.04451	π*	65.90 34.10	4.29	0.78	0.052
LP (1)N_{20} 1.67980	σ	-	BD*(2)C_{22}-O_{23} 0.029952	π*	71.71 28.29	51.89	0.30	0.112
LP (1)O_{23} 1.96859	σ	-	BD*(1)O_{11}-H_{12} 0.03659	σ*	23.58 76.42	3.61	1.17	0.058
LP (1)O_{23} 1.96859	σ	-	BD*(1)N_{20}-C_{22} 0.06556	σ*	37.50 62.50	3.71	1.17	0.059
LP (1)O_{23} 1.96859	σ	-	BD*(1)C_{22}-C_{24} 0.05333	σ*	51.46 48.54	0.97	1.04	0.028
LP (2)O_{23} 1.86818	σ	-	BD*(1)O_{11}-H_{12} 0.03659	σ*	23.58 76.42	7.50	0.75	0.067
LP (2)O_{23} 1.86818	σ	-	BD*(1)N_{20}-C_{22} 0.06556	σ*	37.50 62.50	20.38	0.76	0.111
LP (2)O_{23} 1.86818	σ	-	BD*(1)C_{22}-C_{24} 0.05333	σ*	51.46 48.54	21.22	0.63	0.103
LP (1)O_{28} 1.94881	σ	-	BD* (1)C_{1}-C_{2} 0.03956	σ*	50.72 49.28	3.65	0.90	0.051
LP (1)O_{28} 1.94881	σ	-	BD* (1)C_{1}-C_{13} 0.03877	σ*	49.68 50.32	0.94	0.92	0.026
LP (1)O_{28} 1.94881	σ	-	BD* (1)C_{4}-C_{5} 0.03863	σ*	37.58 62.42	1.63	0.94	0.035
LP (1)O_{28} 1.94881	σ	-	BD* (1)C_{5}-O_{9} 0.03764	σ*	66.92 33.08	3.60	0.90	0.051
LP (1)O_{28} 1.94881	σ	-	BD*(1)C_{13}-H_{39} 0.02518	σ*	66.83 33.17	0.52	1.00	0.020
LP (1)O_{28} 1.94881	σ	-	BD*(1)O_{37}-H_{38} 0.02238	σ*	24.44 75.56	1.28	1.00	0.032
LP (2)O_{28} 1.91688	σ	-	BD* (1)C_{1}-C_{2} 0.03956	σ*	49.68 50.32	3.78	0.67	0.045
LP (2)O_{28} 1.91688	σ	-	BD* (1)C_{1}-H_{33} 0.03884	σ*	38.27 61.73	7.59	0.79	0.069
LP (2)O_{28} 1.91688	σ	-	BD* (1)C_{4}-C_{5} 0.03863	σ*	37.58 62.42	2.95	0.71	0.041
LP (2)O_{28} 1.91688	σ	-	BD* (1)C_{4}-H_{36} 0.01235	σ*	37.45 62.55	0.70	0.77	0.021
LP (2)O_{28} 1.91688	σ	-	BD* (1)C_{5}-C_{6} 0.12449	σ*	46.42 53.58	5.37	0.65	0.053
LP (2)O_{28} 1.91688	σ	-	BD* (1)C_{6}-O_{7} 0.05312	σ*	66.38 33.62	1.89	0.34	0.023
LP (2)O_{28} 1.91688	σ	-	BD*(1)O_{37}-H_{38} 0.02238	σ*	24.44 75.56	2.39	0.77	0.038
LP (1)O_{37} 1.98061	σ	-	BD*(1)C_{1}-C_{13} 0.03877	σ*	49.68 50.32	2.39	0.96	0.043
LP (1)O_{37} 1.98061	σ	-	BD*(1)C_{13}-H_{39} 0.02518	σ*	66.83 33.17	1.08	1.05	0.030

LP (2)O_{37} 1.94810	σ	-	BD*(1)C_1-C_{13} 0.03877	σ*	49.68 50.32	2.87	0.66	0.039
LP (2)O_{37} 1.94810	σ	-	BD* (1)C_2-H_{34} 0.02504	σ*	36.22 63.78	0.63	0.75	0.019
LP (2)O_{37} 1.94810	σ	-	BD*(1)C_{13}-C_{14} 0.04624	σ*	50.22 49.78	7.53	0.66	0.063
LP (2)O_{37} 1.94810	σ	-	BD*(1)C_{13}-H_{39} 0.02518	σ*	66.83 33.17	1.00	0.74	0.024
LP (2)O_{37} 1.94810	σ	-	BD*(1)C_{14}-O_{16} 0.03030	σ*	68.04 31.96	1.93	0.57	0.030
BD(1)C_1-C_2 1.97505	σ	49.28 50.72	BD*(1)C_1-C_{13} 0.03877	σ*	49.68 50.32	1.02	0.98	0.028
BD(1)C_1-C_2 1.97505	σ	49.28 50.72	BD* (1)C_1-H_{33} 0.03884	σ*	38.27 61.73	0.72	1.08	0.025
BD(1)C_1-C_2 1.97505	σ	49.28 50.72	BD* (1)C_2-C_3 0.04675	σ*	47.83 52.17	0.62	0.96	0.022
BD(1)C_1-C_2 1.97505	σ	49.28 50.72	BD* (1)C_2-H_{34} 0.02504	σ*	36.22 63.78	0.73	1.07	0.025
BD(1)C_1-C_2 1.97505	σ	49.28 50.72	BD* (1)C_3-O_{11} 0.02483	σ*	66.47 33.53	1.45	0.92	0.033
BD(1)C_1-C_2 1.97505	σ	49.28 50.72	BD*(1)C_{13}-C_{14} 0.04624	σ*	50.22 49.78	1.90	0.98	0.039
BD(1)C_1-C_2 1.97505	σ	49.28 50.72	BD*(1)N_{20}-C_{22} 0.06556	σ*	37.50 62.50	2.82	1.09	0.049
BD (1)C_1-C_{13} 1.97590	σ	50.32 49.68	BD* (1)C_1-C_2 0.03956	σ*	50.72 49.28	0.80	0.97	0.025
BD (1)C_1-C_{13} 1.97590	σ	50.32 49.68	BD* (1)C_1-H_{33} 0.03884	σ*	38.27 61.73	1.00	1.09	0.029
BD (1)C_1-C_{13} 1.97590	σ	50.32 49.68	BD* (1)C_2-C_3 0.04675	σ*	47.83 52.17	1.82	0.97	0.037
BD (1)C_1-C_{13} 1.97590	σ	50.32 49.68	BD* (1)C_5-O_{28} 0.10041	σ*	69.96 30.04	3.03	0.87	0.046
BD (1)C_1-C_{13} 1.97590	σ	50.32 49.68	BD*(1)C_{13}-C_{14} 0.04624	σ*	50.22 49.78	0.68	0.99	0.023
BD (1)C_1-C_{13} 1.97590	σ	50.32 49.68	BD*(1)C_{13}-H_{39} 0.02518	σ*	37.97 62.03	0.72	1.06	0.025
BD (1)C_1-C_{13} 1.97590	σ	50.32 49.68	BD*(1)C_{14}-C_{15} 0.04028	σ*	49.20 50.80	1.51	0.99	0.035
BD (1)C_1-O_{28} 1.98563	σ	32.74 67.26	BD* (1)C_2-N_{20} 0.02675	σ*	62.16 37.84	0.99	1.15	0.030
BD (1)C_1-O_{28} 1.98563	σ	32.74 67.26	BD* (1)C_5-O_9 0.03764	σ*	66.92 33.08	1.30	1.17	0.035
BD (1)C_1-O_{28} 1.98563	σ	32.74 67.26	BD*(1)C_{13}-H_{39} 0.02518	σ*	37.97 62.03	1.22	1.27	0.035
BD (1)C_1-H_{33} 1.97507	σ	61.73 38.27	BD* (1)C_2-N_{20} 0.02675	σ*	62.16 37.84	0.76	0.85	0.023

BD (1)C_1-H_{33} 1.97507	σ	61.73 28.27	BD* (1)C_2-H_{34} 0.02504	σ*	36.22 63.78	0.72	1.05	0.025
BD (1)C_1-H_{33} 1.97507	σ	61.73 28.27	BD*(1)C_{13}-O_{37} 0.02052	σ*	66.83 33.17	3.67	0.81	0.049
BD (1)C_2-C_3 1.97660	σ	52.17 47.83	BD* (1)C_1-C_2 0.03956	σ*	50.72 49.28	1.08	0.95	0.029
BD (1)C_2-C_3 1.97660	σ	52.17 47.83	BD* (1)C_1-C_{13} 0.03877	σ*	49.68 50.32	1.38	0.97	0.033
BD (1)C_2-C_3 1.97660	σ	52.17 47.83	BD* (1)C_2-H_{34} 0.02504	σ*	36.22 63.78	0.72	1.05	0.025
BD (1)C_2-C_3 1.97660	σ	52.17 47.83	BD* (1)C_3-C_4 0.02430	σ*	50.57 49.43	0.75	0.99	0.024
BD (1)C_2-C_3 1.97660	σ	52.17 47.83	BD* (1)C_4-H_{36} 0.01235	σ*	37.45 62.55	1.41	1.05	0.034
BD (1)C_2-N_{20} 1.98259	σ	37.84 62.16	BD* (1)C_1-O_{28} 0.02939	σ*	67.26 32.74	1.90	1.04	0.040
BD (1)C_2-N_{20} 1.98259	σ	37.84 62.16	BD* (1)C_3-C_4 0.02430	σ*	50.57 49.43	1.06	1.13	0.031
BD (1)C_2-N_{20} 1.98259	σ	37.84 62.16	BD*(1)N_{20}-H_{21} 0.03952	σ*	26.41 73.59	0.52	1.20	0.022
BD (1)C_2-N_{20} 1.98259	σ	37.84 62.16	BD*(1)N_{20}-C_{22} 0.03952	σ*	37.50 62.50	1.38	1.22	0.037
BD (1)C_2-N_{20} 1.98259	σ	37.84 62.16	BD*(1)C_{22}-C_{24} 0.05333	σ*	51.46 48.54	2.63	1.09	0.048
BD (1) C_2-H_{34} 1.97204	σ	63.78 36.22	BD* (1)C_1-H_{33} 0.03884	σ*	38.27 61.73	1.76	0.98	0.037
BD (1) C_2-H_{34} 1.97204	σ	63.78 36.22	BD* (1)C_3-O_{11} 0.02483	σ*	66.47 33.53	1.58	0.81	0.032
BD (1) C_2-H_{34} 1.97204	σ	63.78 36.22	BD* (1)C_3-H_{35} 0.03385	σ*	37.58 62.42	0.70	1.07	0.024
BD (1) C_2-H_{34} 1.97204	σ	63.78 36.22	BD*(1)N_{20}-H_{21} 0.03952	σ*	26.41 73.59	2.78	0.96	0.046
BD (1)C_3-C_4 1.97615	σ	49.43 50.57	BD* (1)C_2-C_3 0.04675	σ*	47.83 52.17	0.62	0.95	0.022
BD (1)C_3-C_4 1.97615	σ	49.43 50.57	BD* (1)C_2-N_{20} 0.02675	σ*	62.16 37.84	1.77	0.93	0.036
BD (1)C_3-C_4 1.97615	σ	49.43 50.57	BD* (1)C_3-H_{35} 0.03385	σ*	37.58 62.42	0.70	1.07	0.024
BD (1)C_3-C41.97615	σ	49.43 50.57	BD* (1)C_4-C_5 0.03863	σ*	49.52 50.48	0.79	0.99	0.025
BD (1)C3-C_4 1.97615	σ	49.43 50.57	BD* (1)C_4-H_{32} 0.01562	σ*	37.46 62.54	0.68	1.05	0.024
BD (1)C_3-C_4 1.97615	σ	49.43 50.57	BD* (1)C_4-H_{36} 0.01235	σ*	37.45 62.55	0.065	1.05	0.023
BD (1)C_3-C_4 1.97615	σ	49.43 50.57	BD* (1)C_5-O_9 0.03764	σ*	66.92 33.08	2.50	0.95	0.044

BD (1)C_3-C_4 1.97615	σ	49.43 50.57	BD*(1)O_{11}-H_{12} 0.03659	σ*	23.58 76.42	1.57	1.07	0.037
BD (1)C_3-O_{11} 1.99204	σ	33.53 66.47	BD* (1)C_1-C_2 0.03956	σ*	50.72 49.28	1.24	1.15	0.034
BD (1)C_3-O_{11} 1.99204	σ	33.53 66.47	BD* (1)C_4-C_5 0.03638	σ*	49.52 50.48	1.66	1.19	0.040
BD (1)C_3-H_{35} 1.9781	σ	62.42 37.58	BD* (1)C_2-N_{20} 0.02675	σ*	62.16 37.84	0.99	0.83	0.026
BD (1)C_3-H_{35} 1.9781	σ	62.42 37.58	BD* (1)C_2-H_{34} 0.02504	σ*	36.22 63.78	1.59	0.95	0.035
BD (1)C_3-C_4 1.97615	σ	49.43 50.57	BD* (1)C_4-H_{32} 0.01562	σ*	37.46 62.54	2.50	0.95	0.043
BD(1) C_4-C5 1.97741	σ	50.48 49.52	BD* (1)C_3-C_4 0.02430		50.57 49.43	0.71	1.01	0.024
BD (1)C4-C_5 1.97741	σ	50.48 49.52	BD* (1)C_3-O_{11} 0.02483	σ*	66.47 33.53	1.90	0.93	0.037
BD (1)C_4-C5 1.97741	σ	50.48 49.52	BD* (1)C_4-H_{32} 0.01562	σ*	37.46 62.54	0.63	1.07	0.023
BD (1)C4-C_5 1.97741	σ	50.48 49.52	BD* (1)C_4-H_{36} 0.01235	σ*	37.45 62.55	0.80	1.07	0.026
BD (1)C_4-C_5 1.97741	σ	50.48 49.52	BD* (1)C_5-C_6 0.12449	σ*	46.42 53.58	0.57	0.96	0.021
BD (1)C_4-C_5 1.97741	σ	50.48 49.52	BD* (1)C_6-O_7 0.05312	σ*	66.38 33.62	1.21	1.19	0.034
BD (1)C_4-C_5 1.97741	σ	50.48 49.52	BD* (1)O_9-H_{10} 0.05186	σ*	22.85 77.15	1.69	1.06	0.038
BD (1)C_4-H_{32} 1.97573	σ	62.54 37.46	BD* (1)C_3-O_{11} 0.02483	σ*	66.47 33.53	1.17	0.79	0.027
BD (1)C_4-H_{32} 1.97573	σ	62.54 37.46	BD* (1)C_3-H_{35} 0.03385	σ*	37.58 62.42	2.25	0.95	0.041
BD (1)C_4-H_{32} 1.97573	σ	62.54 37.46	BD* (1)C_5-C_6 0.012449	σ*	46.42 53.58	4.12	0.82	0.052
BD (1)C_4-H_{32} 1.97573	σ	62.54 37.46	BD* (1)C_5-O_9 0.03764	σ*	66.92 33.08	0.72	0.84	0.022
BD (1)C_4-H_{32} 1.97573	σ	62.54 37.46	BD* (1)C_5-O_{28} 0.10041	σ*	69.96 30.04	0.55	0.74	0.018
BD (1)C_4-H_{36} 1.97433	σ	62.55 37.45	BD* (1)C_2-C_3 0.04675	σ*	47.83 52.17	3.46	0.85	0.048
BD (1)C_4-H_{36} 1.97433	σ	62.55 37.45	BD* (1)C_5-O_{28} 0.10041	σ*	69.96 30.04	4.41	0.75	0.051
BD (1)C_5-C_6 1.98220	σ	53.58 46.42	BD* (1)C_4-C_5 0.03863	σ*	49.52 50.48	0.60	1.00	0.022
BD (1)C_5-C_6 1.98220	σ	53.58 46.42	BD* (1)C_4-H_{32} 0.01562	σ*	37.46 62.54	1.47	1.05	0.035
BD (1)C_5-	σ	33.08	BD* (1)C_1-	σ*	67.26	1.30	1.17	0.035

O_9 1.99130		66.92	O_{28} 0.02939		32.74			
BD (1)C_5-O_9 1.99130	σ	33.08 66.92	BD* (1)C_3-C_4 0.02430		50.57 49.43	1.48	1.25	0.039
BD (1)C_5-O_9 1.99130	σ	33.08 66.92	BD* (1)C_6-O_8 0.5474	π*	66.80 33.20	1.32	1.43	0.039
BD (1)C_5-O_{28}	σ	30.04 69.96	BD* (1)C_1-C_{13} 0.03877	σ*	49.68 50.32	1.47	1.14	0.036
BD (1)C_5-O_{28}	σ	30.04 69.96	BD* (1)C_4-H_{36} 0.01235	σ*	37.45 62.55	1.52	1.22	0.038
BD (1)C_5-O_{28}	σ	30.04 69.96	BD* (1)C_6-O_7 0.05312	σ*	66.38 33.62	1.87	0.80	0.034
BD (1)C_6-O_7	σ	33.62 66.38	BD* (1)C_4-C_5 0.03863	σ*	49.52 50.48	0.83	1.38	0.030
BD (1)C_6-O_7	σ	33.62 66.38	BD* (1)C_6-O_8 0.5474	π*	66.80 33.20	0.58	1.55	0.027
BD (2)C_6-O_7 1.98649	σ	25.54 74.46	BD* (1)C_5-O_{28} 0.10041	σ*	69.96 30.04	2.87	0.60	0.037
BD (2)C_6-O_7 1.98649	σ	25.54 74.46	BD* (2)C_6-O_7 0.37035	σ*	74.46 25.54	2.12	0.37	0.025
BD (1)C_6-O_8 1.99521	σ	33.20 66.80	BD* (1)C_5-O_9 0.03764	σ*	66.92 33.08	0.53	1.33	0.024
BD (1)C_6-O_8 1.99521	π	33.20 66.80	BD* (1)C_6-O_7 0.05312	σ*	66.38 33.62	0.63	1.55	0.029
BD (1)O_9-H_{10}	σ	77.15 22.85	BD* (1)C_4-C_5 0.03863	σ*	49.52 50.48	3.63	1.08	0.056
BD (1)O_9-H_{10}	σ	77.15 22.85	BD* (1)C_4-C_5 0.03863	σ*	49.52 50.48	1.20	1.03	0.031
BD (1)O_{11}-H_{12} 1.98865	σ	76.42 23.58	BD* (1)C_3-C_4 0.02430	σ*	50.57 49.43	2.71	1.10	0.049
BD (1)C_{13}-C_{14} 1.97994	σ	49.78 50.22	BD* (1)C_1-C_2 0.03956	σ*	50.72 49.28	1.91	0.97	0.038
BD (1)C_{13}-C_{14} 1.97994	σ	49.78 50.22	BD* (1)C_1-C_{13} 0.03877	σ*	49.68 50.32	0.63	0.98	0.023
BD (1)C_{13}-C_{14} 1.97994	σ	49.78 50.22	BD*(1)C_{13}-H_{39} 0.02518	σ*	37.97 62.03	0.70	1.06	0.024
BD (1)C_{13}-C_{14} 1.97994	σ	49.78 50.22	BD*(1)C_{14}-H_{31} 0.02469	σ*	37.83 62.17	0.61	1.07	0.023
BD (1)C_{13}-C_{14} 1.97994	σ	49.78 50.22	BD*(1)C_{15}-O_{17} 0.01063	σ*	66.72 33.28	2.03	0.93	0.039
BD (1)C_{13}-C_{14} 1.97994	σ	49.78 50.22	BD*(1)O_{16}-H_{18} 0.04241	σ*	21.87 78.13	0.76	1.07	0.025
BD (1)C_{13}-O_{37} 1.99063	σ	33.17 66.83	BD* (1)C_1-H_{33} 0.03884	σ*	38.27 61.73	1.15	1.28	0.034
BD (1)C_{13}-O_{37} 1.99063	σ	33.17 66.83	BD*(1)C_{14}-O_{16} 0.03030	σ*	68.04 31.96	2.16	1.09	0.043
BD (1)C_{13}-	σ	62.03	BD* (1)C_1-	σ*	67.26	3.46	0.81	0.047

H_{39} 1.97309		37.97	O_{28} 0.2939		32.74			
BD (1)C_{13}-H_{39} 1.97309	σ	62.03 37.97	BD*(1)C_{14}-H_{31} 0.02469	σ*	37.83 62.17	2.38	0.97	0.043
BD (1)C_{13}-H_{39} 1.97309	σ	62.03 37.97	BD*(1)O_{37}-H_{38} 0.02238	σ*	24.44 75.56	2.16	0.96	0.041
BD (1)C_{14}-C_{15} 1.98628	σ	50.80 49.20	BD* (1)C_{1}-C_{13} 0.03877	σ*	49.68 50.32	2.26	0.97	0.42
BD (1)C_{14}-O_{16} 1.99116	σ	31.96 68.04	BD*(1)C_{13}-O_{37} 0.2052	σ*	66.83 33.17	1.55	1.10	0.037
BD (1)C_{14}-H_{31} 1.97902	σ	62.17 37.83	BD*(1)C_{13}-H_{39} 0.02518	σ*	37.97 62.03	2.49	0.96	0.044
BD (1)C_{15}-O_{17} 1.99523	σ	33.28 66.72	BD*(1)C_{13}-C_{14} 0.04624	σ*	50.22 49.78	1.45	1.16	0.037
BD (1)C_{15}-H_{29} 1.98864	σ	60.19 39.81	BD*(1)C_{14}-H_{31} 0.02469	σ*	37.83 62.17	2.36	0.95	0.042
BD (1)C_{15}-H_{30}	σ	61.72 38.28	BD*(1)C_{14}-O_{16} 0.03030	σ*	68.04 31.96	3.86	0.78	0.049
BD (1)C_{15}-H_{30}	σ	61.72 38.28	BD*(1)O_{17}-H_{19} 0.02204	σ*	25.14 74.86	2.35	0.96	0.042
BD (1)N_{20}-H_{21} 1.97752	σ	73.59 26.41	BD* (1)C_{2}-H_{34} 0.02504	σ*	36.22 63.78	1.28	1.12	0.034
BD (1)N_{20}-H_{21} 1.97752	σ	73.59 26.41	BD*(1)C_{22}-O_{23} 0.04451	π*	65.90 34.10	4.00	1.17	0.061
BD (1)N_{20}-H_{21} 1.97752	σ	73.59 26.41	BD*(2)C_{22}-O_{23} 0.29952	π*	71.71 28.29	2.74	0.69	0.039
BD (1)C_{24}-H_{25} 1.98585	σ	62.84 37.16	BD*(1)C_{22}-O_{23} 0.04451	π*	65.90 34.10	2.87	1.06	0.049
BD (1)C_{24}-H_{25} 1.98585	σ	62.84 37.16	BD*(2)C_{22}-O_{23} 0.29952	π*	71.71 28.29	3.40	0.58	0.040
BD (1)C_{24}-H_{26} 1.97519	σ	62.39 37.61	BD*(1)C_{22}-O_{23} 0.04451	π*	65.90 34.10	1.11	1.05	0.031
BD (1)C_{24}-H_{26} 1.97519	σ	62.39 37.61	BD*(2)C_{22}-O_{23} 0.29952	π*	71.71 28.29	4.51	0.57	0.045
BD (1)C_{24}-H_{27} 1.98594	σ	62.39 37.61	BD* (1)N_{20}-C_{22}	σ*	37.50 62.50	3.51	1.02	0.054

$E^{(2)a}$ = energy of hyperconjugation interactions (Stabilization energy in kJ/mol)

E_j-E_i^b = Energy difference (a.u.) between donor and acceptor i and j NBO orbitals

$F^{(i,j)c}$ = the Fock matrix elements (a.u.) between i and j NBO orbitals

σ = Sigma bonding molecular orbital

σ* = Sigma anti-bonding molecular orbital

π = Pi bonding molecular orbital

π^* = Pi anti-bonding molecular orbital

BD = Bonding (2 centers)

BD* = Anti-bonding

CR = Core (1 center)

LP = Lone pair

References

[1] C. N. I. Pang and M. R. Wilkins, *Protein Post-Translational Modification Prediction*, In: Encyclopedia of Bioinformatics and Computational Biology, 15 (2019).

[2] P. Van Damme, K. Hole, A. Pimenta-Marques, K. Helsens, J. Vandekerckhove, R. G. Martinho, K. Gevaert, and T. Arnesen, PLoS Genet **7**, e1002169 (2011).

[3] A. Yokoyama, S. Katsura, R. Ito, W. Hashiba, H. Sekine, R. Fujiki, and S. Kato, Biochem. Biophys. Res. Commun. **410**, 749 (2011).

[4] S. T. Prigge, A. S. Kolhekar, B. A. Eipper, R. E. Mains, and L. M. Amzel, Science (80-.). **278**, 1300 (1997).

[5] S. T. Prigge, R. E. Mains, B. A. Eipper, and L. M. Amzel, Cell. Mol. Life Sci. C. **57**, 1236 (2000).

[6] M. A. Brown and L. M. Stenberg, chapter 9: *Biopharmaceuticals: Post-Translational Modification Carboxylation and Hydroxylation*. Post-translational Modification of Protein Biopharmaceuticals, 209 (2009).

[7] H. Schroten, C. Stapper, R. Plogmann, H. Köhler, J. Hacker, and F.-G. Hanisch, Infect. Immun. **66**, 3971 (1998).

[8] P. Cohen, Trends Biochem. Sci. **17**, 408 (1992).

[9] B. A. Garcia, J. Shabanowitz, and D. F. Hunt, Methods **35**, 256 (2005).

[10] P. Zhang, S. Woen, T. Wang, B. Liau, S. Zhao, C. Chen, Y. Yang, Z. Song, M. R. Wormald, C. Yu, and others, Drug Discov. Today **21**, 740 (2016).

[11] P. de A. G. Redondo, C. V. Nakamura, W. De Souza, and J. A. Morgado-Diaz, J. Histochem. Cytochem. **52**, 629 (2004).

[12] H.-B. Guo, A. Nairn, K. Harris, M. Randolph, G. Alvarez-Manilla, K. Moremen, and M. Pierce, FEBS Lett. **582**, 527 (2008).

[13] S. Hakomori, Proc. Natl. Acad. Sci. **99**, 10231 (2002).

[14] Y. J. Kim and A. Varki, Glycoconj. J. **14**, 569 (1997).

[15] M. Fukuda, Cancer Res. **56**, 2237 (1996).

[16] R. A. Kohnz, L. S. Roberts, D. DeTomaso, L. Bideyan, P. Yan, S. Bandyopadhyay, A. Goga, N. Yosef, and D. K. Nomura, ACS Chem. Biol. **11**, 2131 (2016).

[17] H. Pan, P. Kopečková, J. Liu, D. Wang, S. C. Miller, and J. Kopeček, Pharm. Res. **24**, 2270 (2007).

[18] S. L. Bellis, Biochim. Biophys. Acta (BBA)-Biomembranes **1663**, 52 (2004).

[19] J. Gu and N. Taniguchi, Glycoconj. J. **21**, 9 (2004).

[20] M. M. Fuster and J. D. Esko, Nature Reviews Cancer **5**, 526 (2005).

[21] S. Wang, Y. Wen, Y. Wang, Y. Ma, and Z. Liu, Anal. Chem. **89**, 5646 (2017).

[22] S. Wang, D. Yin, W. Wang, X. Shen, J.-J. Zhu, H.-Y. Chen, and Z. Liu, Sci. Rep. **6**, 22757 (2016).

[23] S. Deshayes, H. Cabral, T. Ishii, Y. Miura, S. Kobayashi, T. Yamashita, A. Matsumoto, Y. Miyahara, N. Nishiyama, and K. Kataoka, J. Am. Chem. Soc. **135**, 15501 (2013).

[24] J. Wang, W. Wu, Y. Zhang, X. Wang, H. Qian, B. Liu, and X. Jiang, Biomaterials **35**, 866 (2014).

[25] A. David, P. Kopecková, J. Kopecek, and A. Rubinstein, Pharm. Res. **19**, 1114 (2002).

[26] N. M. Varki and A. Varki, Lab. Investig. **87**, 851 (2007).

[27] J.-Y. Lee, S.-J. Chung, H.-J. Cho, and D.-D. Kim, Adv. Funct. Mater. **25**, 3705 (2015).

[28] S. Tiwari, B. Tirosh, and A. Rubinstein, Int. J. Pharm. **531**, 281 (2017).

[29] M. J. Frisch, G. W. Trucks, H. B. Schlegel, G. E. Scuseria, M. A. Robb, J. R. Cheeseman, G. Scalmani, V. Barone, B. Mennucci, G. A. Petersson, H. Nakatsuji, M. Caricato, X. Li, H. P. Hratchian, A. F. Izmaylov, J. Bloino, G. Zheng, J. L. Sonnenberg, M. Hada, M. Ehara, K. Toyota, R. Fukuda, J. Hasegawa, M. Ishida, T. Nakajima, Y. Honda, O. Kitao, H. Nakai, T. Vreven, J. A. Montgomery Jr., J. E. Peralta, F. Ogliaro, M. Bearpark, J. J. Heyd, E. Brothers, K. N. Kudin, V. N. Staroverov, R. Kobayashi, J. Normand, K. Raghavachari, A. Rendell, J. C. Burant, S. S. Iyengar, J. Tomasi, M. Cossi, N. Rega, J. M. Millam, M. Klene, J. E. Knox, J. B. Cross, V. Bakken, C. Adamo, J. Jaramillo, R. Gomperts, R. E. Stratmann, O. Yazyev, A. J. Austin, R. Cammi, C. Pomelli, J. W. Ochterski, R. L. Martin, K. Morokuma, V. G. Zakrzewski, G. A. Voth, P. Salvador, J. J. Dannenberg, S. Dapprich, A. D. Daniels, Ö. Farkas, J. B. Foresman, J. V Ortiz, J. Cioslowski, and D. J. Fox, Gaussian Inc. Wallingford CT (2009).

[30] J. P. Perdew, K. Burke, and M. Ernzerhof, *chapter 30*:*Local and Gradient-Corrected Density Functional*, Chemical Applications of Density-Functional Theorys (ACS Publications) **629**, 453 (1996).

[31] V. Barone and M. Cossi, J. Phys. Chem. A **102**, 1995 (1998).

[32] M. S. Jaguar, New York, NY LLC (2017).

[33] M. D. Liptak and G. C. Shields, J. Am. Chem. Soc. **123**, 7314 (2001).

[34] A. D. Bochevarov, M. A. Watson, J. R. Greenwood, and D. M. Philipp, J. Chem. Theory Comput. **12**, 6001 (2016).

[35] M. Kállay and P. R. Surján, J. Chem. Phys. **115**, 2945 (2001).

[36] A. E. Reed and F. Weinhold, J. Chem. Phys. **83**, 1736 (1985).

[37] W. Yang and R. G. Parr, Proc. Natl. Acad. Sci. **82**, 6723 (1985).

[38] P. Jaramillo, P. Pérez, R. Contreras, W. Tiznado, and P. Fuentealba, J. Phys. Chem. A **110**, 8181 (2006).

[39] F. De Vleeschouwer, V. Van Speybroeck, M. Waroquier, P. Geerlings, and F. De Proft, Org. Lett. **9**, 2721 (2007).

[40] R. P. Iczkowski and J. L. Margrave, J. Am. Chem. Soc. **83**, 3547 (1961).

[41] R. K. Roy, V. Usha, J. Paulovic?, and K. Hirao, J. Phys. Chem. A **109**, 4601 (2005).

[42] R. S. Mulliken, J. Chem. Phys. **23**, 10 (1955).

[43] K. Andersson, P. A. Malmqvist, B. O. Roos, A. J. Sadlej and K. Wolinski, J. Phys. Chem. **94**, 5483 (1990).

[44] C.-G. Zhan, J. A. Nichols, and D. A. Dixon, J. Phys. Chem. A **107**, 4184 (2003).

[45] K. H. Min, J.-H. Kim, S. M. Bae, H. Shin, M. S. Kim, S. Park, H. Lee, R.-W. Park, I.-S. Kim, K. Kim, and others, J. Control. Release **144**, 259 (2010).

[46] X. L. Wu, J. H. Kim, H. Koo, S. M. Bae, H. Shin, M. S. Kim, B.-H. Lee, R.-W. Park, I.-S. Kim, K. Choi, and others, Bioconjug. Chem. **21**, 208 (2010).

[47] S. Yourdkhani and M. Jabłoński, J. Comput. Chem. **38**, 773 (2017).

[48] X. Wu, Z. Li, X.-X. Chen, J. S. Fossey, T. D. James, and Y.-B. Jiang, Chem. Soc. Rev. **42**, 8032 (2013).

[49] P. Chen, X. Zhang, L. Jia, R. K. Prud'Homme, Z. Szekely, and P. J. Sinko, J. Control. Release **194**, 341 (2014).

[50] Y. Choi, H. Kim, K. W. Cho, S. R. Paik, H.-W. Kim, K. Jeong, and S. Jung, Carbohydr. Res. **344**, 541 (2009).

[51] A. Lienke, G. Klatt, D. J. Robinson, K. R. Koch, and K. J. Naidoo, Inorg. Chem. **40**, 2352 (2001).

[52] M. Govindarajan and M. Karabacak, Spectrochim. Acta Part A Mol. Biomol. Spectrosc. **96**, 421 (2012).

[53] F.Weinhold and C. R. Landis, *Valency and bonding: a natural bond orbital donor-acceptor perspective*, Cambridge University Press (2005).

[54] A. Choudhary and R. T. Raines, Protein Sci. **20**, 1077 (2011).

[55] A. E. Reed, R. B. Weinstock, and F. Weinhold, J. Chem. Phys. **83**, 735 (1985).

[56] K. C. Gross and P. G. Seybold, Int. J. Quantum Chem. **80**, 1107 (2000).

[57] W. P. Ozimiński and J. C. Dobrowolski, J. Phys. Org. Chem. **22**, 769 (2009).

[58] S. Gunasekaran, S. Kumaresan, R. Arunbalaji, G. Anand, and S. Srinivasan, J. Chem. Sci. **120**, 315 (2008).

[59] G. Socrates, *Infrared characteristics group frequencies*, John Wiley and sons. Ltd: Chichester (1980).

[60] A. Tokatl\i, E. Özen, F. Ucun, and S. Bahçeli, Spectrochim. Acta Part A Mol. Biomol. Spectrosc. **78**, 1201 (2011).

[61] E. Scrocco and J. Tomasi, In Advances in quantum chemistry. Academic Press. **11**, 115 (1978).

[62] F. J. Luque, J. M. López, and M. Orozco, Theor. Chem. Acc. **103**, 343 (2000).

[63] N. Okulik and A. H. Jubert, Internet Electron. J. Mol. Des. **4**, 17 (2005).